6 Summary and Conclusions

Representative carbonate samples were selected from 7 reservoirs across the Middle East Region. Unique rock types were established based on porosity-permeability characteristics, capillary pressure and textural facies. Three main porosity-permeability trends were identified based on textures. Carmen-Kozeny (FZI), Lucia (RFN) and Winland (r35) permeability equations were used to model the experimental data. The following conclusions can be derived from this study,

1. Three porosity-permeability correlations were derived for the 3 main textures by (best-fit) power regression. The power equations can predict permeability with uncertainty factor of +/- 2 (figure 1).
2. Grainy RRT's showed the highest degree of permeability variation within the same porosity range. Muddy samples can be satisfactorily described by a single power correlation.
3. Three FZI trends modelled the porosity-permeability data and honoured the geological textures (figure 11). Permeability can be estimated with a factor of +/- 2 but the samples with the same FZI do not necessarily represent similar flow unit as originally claimed.
4. Three RFN trends modelled the porosity-permeability data and honoured the geological textures (figure 19). For the grainy RRT's, permeability estimation can vary +/- one order of magnitude (a factor of 10) but the prediction is much better for the mixed and muddy RRT's (factor of +/- 2). Samples with same RFN do not necessarily represent similar flow unit.
5. Winland r35 trends poorly modelled the experimental data (figure 23) and did not conform to the texture-based correlations.

The authors wish to acknowledge the support from Abu Dhabi National Oil Company (ADNOC) and Ingrain - Halliburton.

References

1. S.K. Masalmeh and X.D. Jing, The Importance of Special Core Analysis in Modelling Remaining Oil Saturation in Carbonate Fields, SCA2008-03 (2008)
2. M. Dernaika, Z. Kalam, S. Skjaeveland, Understanding Imbibition Data in Complex Carbonate Rock Types, SCA2014-59 (2014)
3. J.J.M. Buiting, E.A. Clerke, Permeability from porosimetry measurements: Derivation for a tortuous and fractal tubular bundle, J Petrol Sci Eng, (2013) http://dx.doi.org/10.1016/j.petrol.2013.04.016i
4. M.R. Dernaika, Y. Naseer Uddin, S. Koronfol, O. Al Jallad, G. Sinclair, Multi-Scale Rock Analysis for Improved Characterization of Complex Carbonates, SCA2015-034 (2015)
5. M.R. Dernaika, B. Mansour, D. Gonzalez, S. Koronfol, F. Mahgoub, O. AlJallad, M. Contreras, Upscaled Permeability and Rock Types in a Heterogeneous Carbonate Core from the Middle East, SPE-185991-MS (2017)
6. M.R. Dernaika, and G.G. Sinclair, Resolving the Link between Porosity and Permeability in Carbonate Pore Systems, SCA2017-77 (2017)
7. M. Mousavi, M. Prodanovic, and D. Jacobi, New Classification of Carbonate Rocks for Process-Based Pore-Scale Modeling, SPE 163073, SPE J. (2013)
8. R.J. Dunham, Classification of Carbonate Rocks According to Depositional Texture. In Classification of Carbonate Rocks: A Symposium. American Association of Petroleum Geologists Memoir 1, ed. W.E. Ham, 108-121. Tulsa, Oklahoma: AAPG (1962)
9. H. Al-Owihan, M. Al-Wadi, S. Thakur, S. Behbehani, N. Al-Jabari, M. Dernaika, and S. Koronfol, Advanced Rock Characterization by Dual-Energy CT Imaging: A Novel Method for Complex Reservoir Evaluation, IPTC 17625 (2014)
10. M.R. Dernaika, B. Mansour, O. AlJallad, Characteristics of Carbonate Rock Types in the Middle East, SCA2018-65 (2018)
11. S. Serag El Din, M.R. Dernaika, M.Z. Kalam, and L. Hannon, The Effect of Rock Properties on Residual Oil Saturation in Heterogeneous Carbonate Rocks, SPE-164141 (2013)
12. S.K. Masalmeh and X.D. Jing, Improved Characterization and Modelling of Carbonate Reservoirs for Predicting Waterflood Performance, IPTC-11722-MS (2007)
13. J.O. Amaefule, M. Altunbay, D. Tiab, D.G. Kersey, and D.K. Keelan, Enhanced Reservoir Description: Using Core and Log Data to Identify Hydraulic (Flow) Units and Predict Permeability in Uncored Intervals/Wells, SPE 26436 (1993)
14. A.K. Ambastha, and T.J. Moynihan, A Simple And Accurate Method For An Integrated Analysis Of Core And Log Data To Describe Reservoir Heterogeneity, Petroleum Society of Canada. doi:10.2118/96-01-06 (1996)
15. J. Kozeny, Uber Kapillare Leitung des Wassel'S im Boden, Sitzungsberichte, Royal Academy of Science, Vienna, Proc. Class I **136**, 271-306 (1927)
16. P.E. Carmen, Fluid Flow through Granular Beds, Trans. AIChE **15**, 150 -166 (1937)
17. J.W. Jennings, and F.J. Lucia, Predicting Permeability From Well Logs in Carbonates With a Link to Geology for Interwell Permeability Mapping, SPE-84942 (2003)
18. S. Kolodzie, Analysis of Pore Throat Size And Use of the Waxman-Smits Equation To Determine OOIP in Spindle Field, Colorado, SPE 9382 (1980)
19. A.J. Martin, S.T. Solomon, and D.J. Hartmann, Characterization of Petrophysical Flow Units in Five Carbonate Reservoirs. American Association of Petroleum Geologists Bull. 81 (5):734 (1997).

Direct Magnetic Resonance Measurement of Average Pore Size

Florin Marica[1], *Armin* Afrough[2], *Derrick* Green[3], *Laura* Romero-Zeron[4], and *Bruce* Balcom[1,*]

[1]Department of Physics, University of New Brunswick, Fredericton, New Brunswick, E3B 5A3, Canada
[2]Centre for Oil and Gas - DTU, Technical University of Denmark, Kgs. Lyngby 2800, Denmark
[3]Green Imaging Technologies, Fredericton, New Brunswick, E3A 8V2, Canada
[4]Department of Chemical Engineering, University of New Brunswick, Fredericton, E3B 5A3, Canada

Abstract. Magnetic Resonance relaxation time distribution measurements, notably T_2 measurement, are commonly employed as a proxy measurement of pore size. They are not direct measurements of pore size and may only be converted to pore size through a separate determination of a relaxivity. In this work we employ the Brownstein-Tarr interpretation of magnetic resonance relaxation to identify non-ground modes of signal decay. These modes, most readily identified through a T_1-T_2 measurement, permit determination of an average pore size and surface relaxivities ρ_1 and ρ_2. Bulk pore size measurements are reported for three different sandstones with average pore size confirmed by electron microscopy. The pore size measurement may be spatially resolved with a spatially resolved T_1-T_2 measurement, implemented with an inversion recovery preparation for an SE-SPI T_2 mapping measurement. Spatially resolved pore size measurements agree with bulk measurements.

1 Introduction

Pore size is one of the most basic core analysis measurements. In principal magnetic resonance (MR) is ideally suited to such a measurement given sensitivity of the MR signal lifetimes to pore size through surface relaxation. A surface bound fluid layer in rapid exchange with a bulk like volume is assumed to yield an average MR signal lifetime that is proportional to the pore size. A distribution of lifetimes is thus a useful proxy for the pore size distribution [1]. Such lifetimes however require a separate calibration of surface relaxivity to permit conversion to a pore size with conventional units of size.

We have recently found that the Brownstein-Tarr approach [2] to interpreting MR relaxation rates permits a determination of average pore size in brine saturated core plugs [3,4]. The Brownstein-Tarr approach considers the competition between surface relaxation and diffusion within a pore and predicts multi-modal relaxation decay for T_1 and T_2 even for single pores. Multi-modal relaxation decay manifests itself as multiple signal lifetimes in a conventional relaxation experiment. Identifying and discriminating the ground mode signal lifetimes and the non-ground mode signal lifetimes is problematic in a conventional 1D relaxation experiment where realistic porous media have a distribution of lifetimes due to a distribution of pore sizes, in addition to short signal lifetime components due to clay bound water and other features.

Multi-modal relaxation in MR, according to the Brownstein-Tarr theory, has been recognized and understood for many years [5]. Song has emphasized the use of internal gradients to modify the non-ground mode signals [6]. The opportunity for exploiting non-ground modes to determine pore size has not been realized prior to our work.

Identifying and discriminating the ground and non-ground modes is easier in a 2D T_1-T_2 relaxation correlation experiment as described in this work. The T_1-T_2 experiment has found great utility in core analysis through its ability to discriminate molecular species [7], discriminate pore environments [8] and in more sophisticated interpretations, to measure wettability [9]. In previous work we have developed an adiabatic slice selective approach to a spatially resolved T_1-T_2 measurement [10].

Our goals in this paper are three-fold: (i) to introduce the average pore size measurement to the core analysis community, (ii) to test the measurement through application to a range of samples and (iii) to introduce a spatially resolved measurement of the pore size.

2 Theory

Magnetization evolution due to translational motion of spins in magnetic fields is governed by the Bloch-Torrey equations [11]. Brownstein and Tarr [2] examined the solution of these equations under conditions when diffusion does not necessarily result in uniform magnetization evolution in the pore. The Brownstein-Tarr number BT_i describes the ratio of the relaxation rate at pore boundaries to the rate of diffusion in a confined geometry.

$$\mathrm{BT}_i = \frac{\rho_i l}{D} \tag{1}$$

* Corresponding author: bjb@unb.ca

The index i in Eq. 1 discriminates between spin lattice relaxation, i = 1, with a T_1 time constant and spin-spin relaxation, i = 2, with a T_2 time constant. D is the molecular diffusion coefficient, ρ_ι is the surface relaxivity while l is the confinement length or pore size. Confinement length is a more general description that recognises the possibility that a pore may be only partially filled by the wetting fluid and it recognizes the possibility that a more complicated pore geometry does not permit a simple descriptor of pore size. In this work we will refer to l as the pore size.

Brownstein and Tarr identified three regimes of behaviour based on BT_i. $BT_i << 1$ is the fast diffusion regime. In this regime magnetization in the pore space is uniform and exchange between water at the pore surface and bulk like water in the pore centre is rapid. In this limit the observed relaxation rate depends on the pore surface to volume ratio. We note that this regime is almost universally assumed in MR petrophysics. This regime is also the rapid exchange regime of Zimmerman and Brittin [12]. $BT_i >> 10$ is the slow diffusion regime. The observed relaxation rate depends strongly on diffusion since diffusion to the pore surface is the limiting step. In this regime the relaxation behaviour depends weakly on surface relaxivity in higher order modes. The intermediate regime $1< BT_i<10$ is common in porous media and the observed relaxation behaviour depends on both surface relaxivity and diffusion.

The experimental data, transverse magnetization m_+, resulting from a 2D T_1-T_2 measurement is given by Eq. 2. In this equation τ_1 is a time period of signal evolution with T_1 encoding, while τ_2 is a time period of signal evolution with T_2 encoding.

$$m_+(\tau_1,\tau_2) = \int_{\boldsymbol{r}} M_+(\boldsymbol{r},\tau_1,\tau_2)\, d\boldsymbol{r} = \sum_{q=0}^{\infty}\sum_{p=0}^{\infty} I\left(T_{1,p},T_{2,q}\right) e^{-\tau_1/T_{1,p}} e^{-\tau_2/T_{2,q}} \quad (2)$$

The experimental goal is to determine the 2D correlation function $I(T_{1,p}, T_{2,q})$ through inverse Laplace transformation as described in the next section. $I(T_{1,p}, T_{2,q})$ maps signal intensity to different T_1 and T_2 coordinates with p and q indexing the mode with p,q = 0 representing the ground mode and p,q = 1 representing the first non-ground mode. The BT_i number determines whether significant populations exist in the non-ground mode. In simple geometries, and for arbitrary BT_i values, the eigenvalues of signal lifetime for ground and non-ground modes are given by Eq. 3.

$$T_{i,n} = \frac{l^2}{4D\,\xi_{n,i}^2} \quad (3)$$

where $\xi_{n,i}$ are functions of confinement geometry, diffusion coefficient, eigenvalue number n, and BT_i. In a planar pore geometry $\xi_{n,i}$ are the positive roots of Eq. 4 [2].

$$2\xi_{n,i}\tan\xi_{n,i} = BT_i \quad (4)$$

Eqs. 1, 3 and 4, adapted from Brownstein-Tarr [2], are valid for planar pore geometries for both ground $n = 0$ and non-ground $n > 0$ eigenvalues and for longitudinal $i = 1$ and transverse $i = 2$ relaxation processes. These equations, with pore size l, and relaxivities ρ_1, ρ_2 determine the experimental peak locations in T_1-T_2 experiments.

This analysis yields a single pore size, rather than a distribution of pore sizes, which we interpret as an average pore size. The effect of pore shape does not significantly affect eigenvalues, and their intensities, for magnetic resonance relaxation in porous media. This is especially true for $BT_i \ll 100$ [2].

3 Experimental

The bulk T_1-T_2 measurement was a conventional inversion recovery followed by a variable T_1 recovery period with a CPMG spin echo train read out, as described by Eq. 5.

$$\underbrace{\left[\pi - \tau_1 - \frac{\pi}{2}\right]}_{T_1 \text{ encoding}} \underbrace{\left[-(\tau_i - \pi - \tau_i)_N\right]}_{T_2 \text{ encoding}} \quad (5)$$

The echo train data acquired is described by Eq. 2. A regularized inverse two-dimensional Fredholm integral of the first kind transforms the measured signal $m_+(\tau_1,\tau_2)$ into a 2D relaxation correlation function $I\left(T_{1,p},T_{2,q}\right)$ from which eigenvalues of magnetic resonance relaxation may be identified. This process is more commonly described as a 2D inverse Laplace transform. The inversion algorithm of Venkataramanan [13] was employed in this work. Increasing the regularization parameter α leads to smooth solutions whereas small α leads to a discretized result. A large regularization parameter, $\alpha = 1000$, was employed to identify the dominant ground mode peak. The regularization parameter was systematically decreased, usually to $\alpha = 0.1$ to yield a discretized result from which the first non-ground mode can be identified. A direct search optimization method [14] varied $\log_{10} l/\mu\text{m}$, $\log_{10} \rho_1/(\mu\text{m}/s)$, and $\log_{10} \rho_2/(\mu\text{m}/s)$ and solved Eqs. 1, 3 and 4, to match the time constants of eigenvalues detected in $I\left(T_{1,p},T_{2,q}\right)$.

Bulk T_1-T_2 MR measurements were performed on a 8.59 MHz Maran DRX-HF imaging system (Oxford Instruments, Abingdon, UK), equipped with a 1000-watt RF amplifier (Tomco Technologies, Stepney, Australia), AE Techron 7782 gradient amplifiers (AE Techron, Elkhart, IN) and water cooled gradient coils. The 44 mm inner diameter custom-built RF probe provided 90° RF pulses with a duration of 10.6 μs for an input RF power of 300 W. The basic experiment was repeated for 55 inversion recovery delays, spanning 500 usec to 1.9 sec. The echo time was 1 msec with 21 time domain points collected at the echo peak for signal averaging. Sixteen signal averages were collected for an overall experimental time of almost one hour. The peak SNR in the T_1-T_2 data set was more than 600.

The spatially resolved T_1-T_2 measurement was performed on a 2.21 MHz Maran DRX2 imaging system (Oxford Instruments, Abingdon, UK), equipped with a

25-watt RF amplifier and 1D vertical gradient coil. The 43 mm inner diameter probe provided 90° RF pulses with a duration of 28.5 μs. The basic experiment was repeated for 53 inversion recovery delays, spanning 100 usec to 10 sec. The first and subsequent echo times were 1 msec with sixteen time domain data points collected at the each echo peak for signal averaging. Four signal averages, each requiring 19 minutes, were collected for 16 k-space data points, yielding a final image of 16 pixels.

The samples under test, Buff Berea, Nugget, and Castlegate sandstones for bulk measurements, and Berea sandstone and Indiana limestone for spatially resolved measurement, were purchased from Kokurek Industries (Caldwell, TX). All samples had a diameter of 38 mm and were saturated with a 2% (w/v) solution of NaCl in distilled water. The Buff Berea, Nugget, and Castlegate sandstone core plugs were 50 mm in length, whereas the Berea sandstone and Indiana limestone core plugs were cut to 25 mm length to form a composite 1D sample of 50 mm length.

Natural drying was minimized by wrapping the core plugs with Teflon tape and a plastic film. The samples were maintained at 23 ºC during data acquisition.

4 Results and Discussion

Experimental bulk T_1-T_2 results are reported in Figs. 1-3 for brine saturated Buff Berea, Castlegate and Nugget sandstones. For each sample the three-part figure shows the T_1-T_2 distribution determined by inversion with three levels of regularization. The coarsest result, $\alpha = 1000$, permits one to identify the ground mode and its T_1, T_2 coordinates. The dominant ground mode peak is vulnerable to pearling with small values of the regularization parameter but non-ground mode peaks are not distorted by pearling. The first non-ground mode is typically less than ten percent of the intensity of the ground mode, with the second ground mode reduced still further in intensity. In some samples the second ground mode is clearly observable experimentally, but not in the data reported here. The intensity data of the non-ground modes is not at present incorporated into the data analysis. Only their lifetime coordinates are employed in the analysis.

The T_1 T_2 coordinates of the modes are connected by the pore size l, and the relaxivities ρ_1 and ρ_2 in Eqs 1, 3 and 4. Thus identifying the position of the modes permits determination of these three parameters through the optimization described above. The T_1 T_2 coordinates of the first non-ground mode, determined by optimization, are often displaced somewhat from the experimentally identified peak. The optimization process is more robust than might be imagined in part because there is a physical reality to the pore size l and the relaxivities ρ_1 and ρ_2. Values of these parameters which are too large or too small after optimization suggest a need to iterate the procedure.

Exploring the robustness of this measurement and process requires measurement of multiple samples. In the current study we focused on three similar but different sandstones as an experimental check on these procedures. Note that in each sample the T_1-T_2 data points, both experimental and predicted by optimization in Figs. 1-3, are very similar. The derived pore sizes and relaxivities are reported in Table 1 below.

Table 1: Pore size and relaxivities of samples studied.

Sample	Pore size l, um	ρ_1 , um/sec	ρ_2 , um/sec
Buff Berea	21	130	390
Castlegate	29	150	400
Nugget	27	175	1000

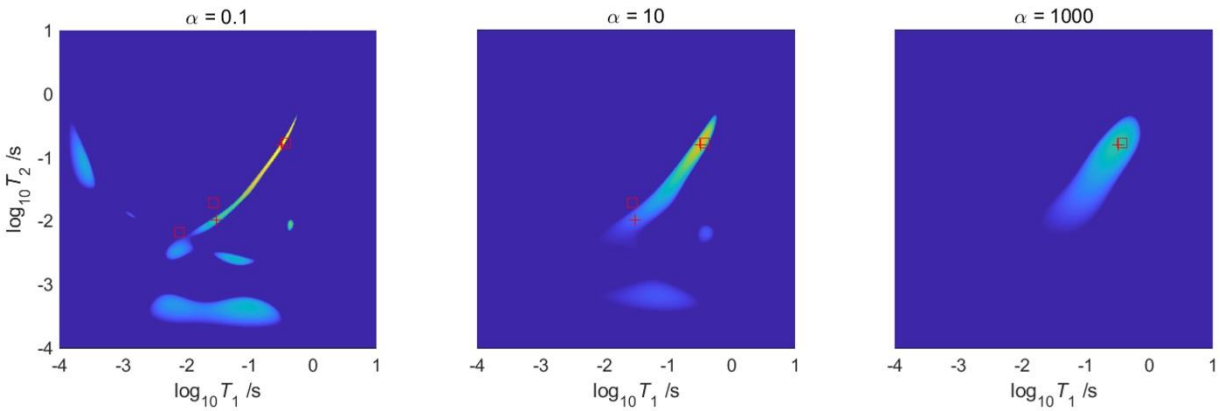

Figure 1: T_1-T_2 results for Buff Berea sandstone processed with three different values of the regularization parameter. The red crosses identify the experimental peaks of interest, the red boxes are calculated results. The peak at the longest lifetimes is the dominant ground

mode peak. The box at intermediate lifetimes identifies the first non-ground mode. The box at the shortest lifetimes is a prediction for the second non-ground mode. The display scale is logarithmic to reveal low intensity peaks.

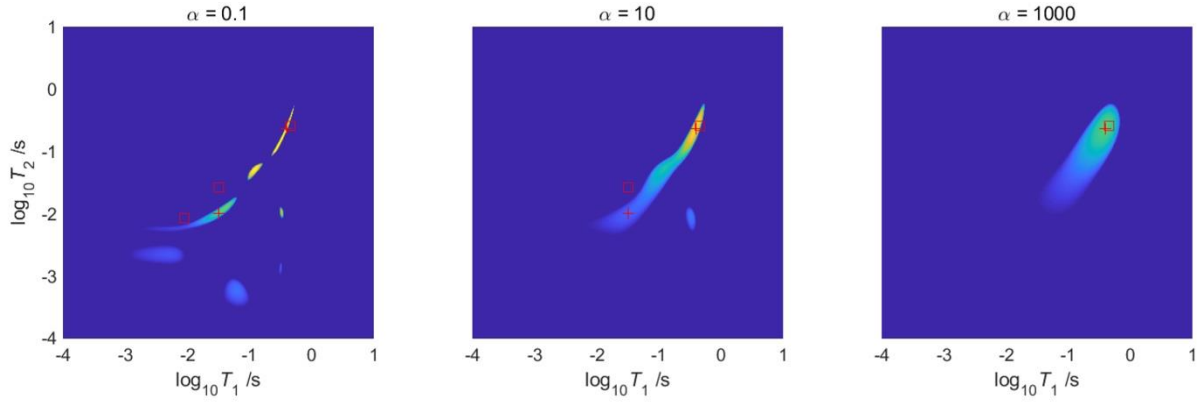

Figure 2: T_1-T_2 results for the Castlegate sandstone processed with three different values of the regularization parameter. Other descriptions are as per Figure 1.

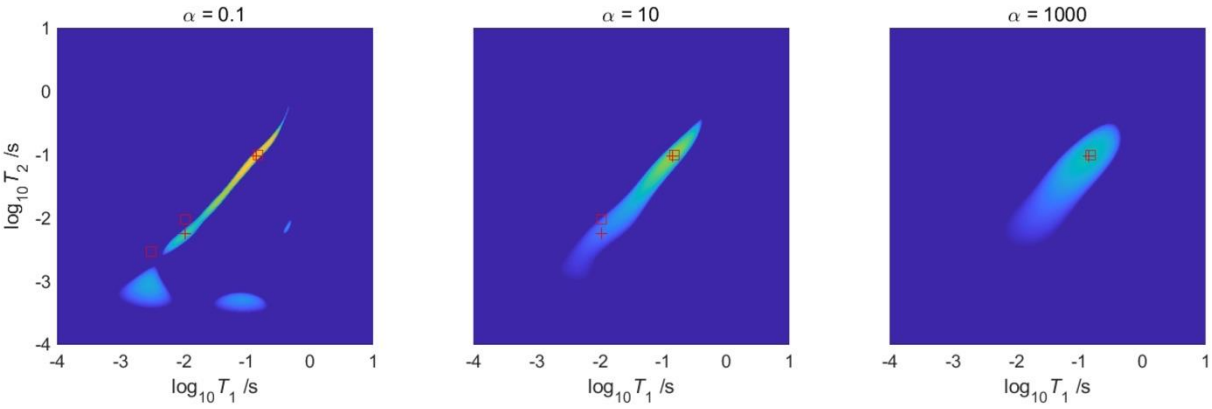

Figure 3: T_1-T_2 results for Nugget sandstone at three different values of the regularization parameter. Other parameters and descriptions are as per Figure 1.

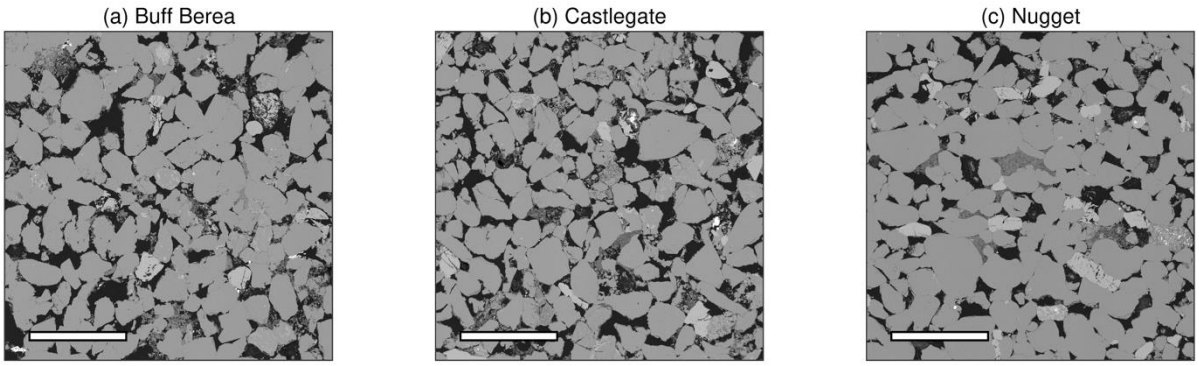

Figure 4: Backscattered SEM images of resin-impregnated sandstones, with polished surfaces. The scale bar in each image indicates 500 um. The resin-filled pore space is black, quartz is medium gray, feldspar is light gray, while clay is dark gray.

The pore sizes and relaxivities of the samples reported in Table 1, in combination with the self-diffusion coefficient of water, show that all three samples exist in the intermediate regime of Brownstein-Tarr theory. T_1-T_2 derived pore sizes may be checked by ground truth electron microscopy measurements. This is critical to the validation process for this new measurement. Thin section backscattered SEM images, Fig. 4, were acquired for each of the three sandstone samples. The images show a very similar pore structure for the three samples, with average pore sizes determined to be 40 um, 35 um and 37 um for the Buff Berea, Castlegate and Nugget samples. These are very similar one to another, and they match within a factor of 2 the T_1-T_2 derived values for each sample. There is no

evidence for two dominant pore sizes in the T_1-T_2 results. The SEM results confirm the pore size is single modal. Two dominant pore sizes are revealed in T_1-T_2 results by two ground mode peaks, visible even with a large regularization parameter [3].

The surface relaxivities reported in Table 1 are substantially larger, by more than an order of magnitude, than those reported by other investigators [15-17]. The minimization procedure to determine pore size and relaxivities in the Brownstein-Tarr analysis is more sensitive to the pore size that to relaxivity. The significant and systematic difference from literature values suggests however a more fundamental reason for the difference. The assumption of a planar pore geometry, as opposed to a spherical geometry, will play a role, but we believe the differences are related to the assumptions employed in the conventional determination of relaxivity as compared to the new measurement.

The Brownstein-Tarr modal analysis, and observation of non-ground modes in these experiments, is based on the combined effect of diffusion and surface relaxivity in determining the rate of change of observable magnetization. The combined effect of size, diffusion and surface relaxation is manifest in Eqs. 1,3,4. The conventional approach to determining surface relaxivity assumes rapid diffusional exchange in the pore space, and the rate of change of observable magnetization depends solely on size (S/V) and surface relaxivity. An independent measurement of S/V permits determination of ρ in the conventional approach. If fluid in the pore is not in the rapid diffusion limit, and the change in observable magnetization depends on diffusion of fluid to the pore surface, the determination of ρ will be in error and the estimated value in the conventional analysis will be low. The quantitative differences in ρ anticipated in the two approaches will be the subject of future investigation. It is certainly true that the surface relaxivity determined through a BT analysis, assuming diffusion is important, should not be employed in the conventional analysis to determine pore size.

The utility of the T_1-T_2 measurement for various purposes has suggested the merits of developing a spatially resolved T_1-T_2 measurement. Our initial work in this area led to a slice selective method referred to above [10]. The SE SPI method developed at UNB some years ago [18] has been very successful in measurements of spatially resolved T_2 distributions. As an alternative to a slice selective regional T_1-T_2 we now introduce a simple modification of the SE SPI measurement through prepending an inversion pulse and variable T_2 recovery delay to the SE SPI method to permit T_1-T_2 profiling. This pulse sequence is illustrated in Fig. 5. In order to reduce the measurement time we limit the number of k-space data points encoded to sixteen, and thus reduce the number of image data points to sixteen as well. Spatial encoding occurs through signal phase imparted by the phase encoding gradient applied after the first 90° pulse, following partial M_z recovery. The first echo in the echo train often has a longer echo time to permit gradient turn-on and turn-off in the first τ_i interval.

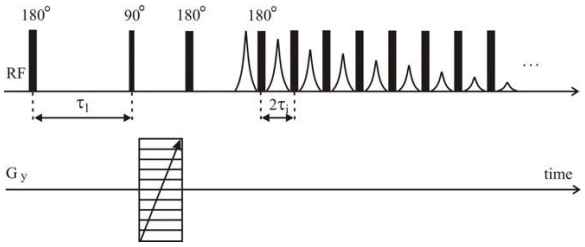

Figure 5: Inversion prepared SE SPI T_1-T_2 mapping profile measurement.

The spatially resolved T_1-T_2 weighted data sets may be processed, pixel by pixel, to yield a space resolved estimate of the pore size, via the procedures described above for bulk measurement. To test this methodology, and the analogous processing, a composite test phantom was created from half-length Berea and Indiana limestone core plugs. These fully brine saturated samples were then subjected to the inversion recovery SE SPI measurement of Fig. 5.

One T_1-T_2 weighted data set is reproduced as Fig. 6. In this data set we have position, 16 pixels, as the horizontal x axis. The image intensity is the vertical axis while the T_2 decay is manifest as an attenuation of the core plug profiles in the time dimension which is echo time multiplied by the echo number. This particular data set was acquired with a long τ_1 value such that M_z magnetization is fully recovered at the commencement of the echo train. This makes it easier to make physical sense of the T_2 weighted profiles that are generated for the two core plugs in the field of view. This data set is just one of 53 T_1 weighted data sets acquired during the measurement.

The data were analysed to yield a space resolved pore size within the two core plugs. The space resolved pore size measurement worked well, yielding a pore size of 24 um for the Berea and 53 um for the Indiana limestone. Previous bulk T_1-T_2 measurements revealed a pore size of 22 um for the Berea sample, with an SEM derived pore size of 26 um [3]. Similar bulk T_1-T_2 measurements of the Indiana limestone revealed a bimodal pore size distribution with large pores of 40 um and small pores of 10 um [3]. Complementary SEM images revealed large pores of 50 um and 10 um. The space resolved T_1-T_2 measurement does not observe the small pore size range in the Indiana limestone sample. The reasons for this discrepancy are under investigation, but probably relate to the difficulty of observing the short lifetime first non-ground mode signal in the imaging data. Nevertheless, the space resolved results are in remarkable agreement and

certainly suggest the merit of analysing experimental

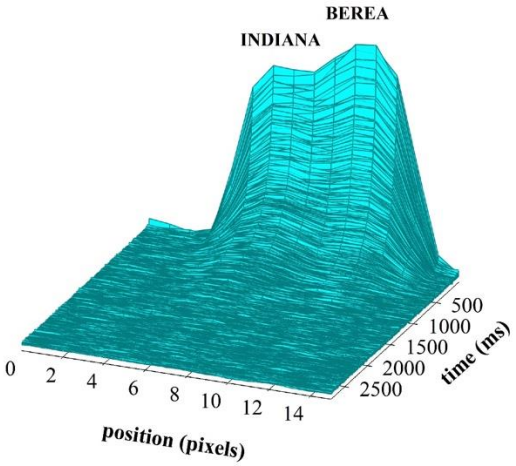

Figure 6: SE SPI based T_1-T_2 mapping profile series of a composite Berea sandstone and Indiana limestone phantom. The τ_1 for this data set was 9 seconds, ensuring full M_z recovery and no T_1 weighting of the individual profiles.

systems where the pore occupancy and thereby confinement length will vary with position. The prolonged acquisition time of the space resolved measurement, at present, will limit measurement to systems which are in a steady state. Measurement at higher fields will of course improve the sensitivity, at the expense of potentially altering the transverse relaxation rate due to diffusion through internal field gradients.

5 Conclusion

We have shown the application of a new T_1-T_2 measurement of average pore size to a range of sandstone samples. In accord with Brownstein-Tarr theory, non-ground modes will also appear in one dimensional relaxation experiments, but we believe non-ground modes will be easier to identify in two-dimensional experiments.

While a sophisticated data analysis stage is required, data processing is nevertheless robust. Automating the data processing is a clear goal but will require experience with a still larger cohort of samples. Future work will also explore the quantitative difference in relaxivities predicted by the new approach in comparison to a conventional analysis. If diffusion in the pore space is a common limitation on the observed relaxation rate then it is apparent that conventional estimates of relaxivity may be low as opposed to the current estimates being high.

We have also introduced a new spatially resolved T_1-T_2 measurement which is general in application, but which has particular utility for space resolved pore size measurements via the procedures described in this paper.

The authors thank NSERC of Canada for a Discovery grant and the Canada Chairs program for a Tier 1 chair in MRI of Materials.

6 References

1. G. Coates, L. Xiao, M. Prammer, *NMR Logging: Principles and Applications.* Houston TX, USA: Halliburton Energy Services, 1999.

2. K. Brownstein and C. Tarr, “Importance of Classical Diffusion in NMR Studies of Water in Biological Cells” *Phys. Rev. A*, vol. 19, no. 6, 2446-2453, 1979.

3. A. Afrough, S. Vashaee, L. Romero-Zeron, and B. Balcom, “Absolute Measurement of Pore Size based on Nonground Eigenstates in Magnetic Resonance Relaxation” *Phys. Rev. Appl*., vol. 11, 2019, Art. no. 041002.

4. A. Afrough, “Magnetic Resonance Imaging of Enhanced Oil Recovery Processes in Porous Rocks” Ph.D. Dissertation, Dept. Chem. Eng., U. New Brunswick, Fredericton NB, Canada, 2019.

5. D. J. Wilkinson, D. L. Johnson and L. M. Schwartz, “Nuclear Magnetic Relaxation in Porous Media: The role of mean lifetime τ(ρ,D)” *Phys. Rev. B*, vol. 44, no. 10, 4960-4973, 1991.

6. Y.-Q. Song, “Detection of the High Eigenmodes of Spin Diffusion in Porous Media” *Phys. Rev. Lett.,* vol. 85, 3878-3881 (2000).

7. M. Fleury and M. Romero-Sarmiento, “Characterization of shales using T_1–T_2 NMR maps” *J. Pet. Sci. Eng.,* vol. 137, 55-62, 2016.

8. Y.-Q. Song, L. Venkataramanan, M. Hurlimann, M. Flaum, P. Frulla and C. Straley, “T_1–T_2 Correlation Spectra Obtained Using a Fast Two-Dimensional Laplace Inversion” *J. Magn. Reson.,* vol. 154, 261-268 2002.

9. A. Valori and B. Nicot, “A Review of 60 Years of NMR Wettability” Society of Core Analysts, Trondheim Norway, August 2018, Art. no. 017.

10. S. Vashaee, M. Li, B. MacMillan, F. Marica, H. Kwak, J. Gao, A. Al-harbi and B. Balcom, “Local T_1-T_2 distribution measurements in porous media” *J. Magn. Reson.,* vol. 287, 113-122, 2018.

11. H. Torrey, “Bloch Equations with Diffusion Terms” *Phys Rev.* vol. 104, no. 3 ,563-565, 1956.

12. J. R. Zimmerman and W.E. Brittin, “Nuclear Magnetic Resonance Studies in Multiple Phase Systems: Lifetime of a Water Molecule in an

Adsorbing Phase on Silica Gel" *J. Phys. Chem.,* vol. 61, no. 10, 1328-1333, 1957.

13. L. Venkataramanan, Y.-Q. Song and M. Hurlimann, "Solving Fredholm integrals of the first kind with tensor product structure in 2 and 2.5 dimensions" *IEEE Trans. Signal Process.,* vol. 50, no. 5, 1017-1026, 2002.

14. T. Kolda, R. Lewis and V. Torczon, "Optimization by Direct Search: New Perspectives on Some Classical and Modern Methods" *SIAM Rev.,* vol. 45, no. 3, 385-482, 2003.

15. M. D. Hurlimann, K. G. Helmer, L. L. Latour and C. H. Sotak, "Restricted Diffusion in Sedimentary Rocks. Determination of Surface-Area-to-Volume Ratio and Surface Relaxivity" *J. Magn. Reson. A,* vol. 111, 169-178, 1994.

16. M. Fleury, "NMR Surface Relaxivity Determination using NMR Apparent Diffusion Curves and BET Measurements" Society of Core Analysts, Calgary, Canada, September 2017, Art. no. 035.

17. Z, X. Liao, J. Paulsen and Y.Q. Song, "Robust Determination of Surface Relaxivity from Nuclear Magnetic D-T_2 Measurements" *J. Magn. Reson.,* vol. 259, 146-152, 2015.

18. O. Petrov, G. Ersland and B. Balcom, "T_2 distribution mapping profiles with phase-encode MRI"
J. Magn. Reson., vol. 209, 39-46, 2011.